Available online at www.sciencedirect.com
SCIENCE DIRECT®
Journal of Solid State Chemistry 177 (2004) 3052–3057
JOURNAL OF SOLID STATE CHEMISTRY
http://elsevier.com/locate/jssc

Effect of varying the acid to metal ion ratio R on the structural and magnetic properties of SiO_2-doped Ni–Zn ferrite

K.H. Wu* and W.C. Huang

Department of Applied Chemistry, Chung Cheng Institute of Technology, NDU, Ta-Hsi, Taoyuan 33, Taiwan, ROC

Received 25 March 2004; received in revised form 10 May 2004; accepted 12 May 2004

Available online 24 June 2004

Abstract

A nitrate–citrate–silica gel was prepared from metallic nitrates, citric acid and tetraethoxysilane (TEOS) by sol–gel process with different citric acid to metal nitrates ratio R, and it was further used to synthesize $Ni_{0.5}Zn_{0.5}Fe_2O_4/20$ wt% SiO_2 nanocomposites by auto-combustion. The effect of varying the citric acid to metal nitrates ratio R on the structural and magnetic properties of the composites were studied by IR, ^{29}Si CP/MAS NMR, XRD, EPR and SQUID measurements. The nitrate–citrate–silica gels exhibited self-propagating combustion behavior, and it directly transformed into nanosized (14–22 nm) NiZn ferrite particles with spinel crystal structure after combustion. The R value in the starting solution affects the magnetic interaction between NiZn ferrite and silica, and then determines the particle size. Further, varying the R value has a direct effect on the EPR parameters (ΔH_{PP}, g factor, N_S and T_2) and SQUID parameters (M_s, M_r and H_c) of the as-synthesized powder.

Keywords: Sol–gel; Ferrite; Silica; EPR; Squid

1. Introduction

NiZn ferrites are one of the most versatile magnetic materials for general use, which have many applications in both low and high frequency devices and play a useful role in many technological applications such as microwave devices, power transformers in electronics, rod antennas, read/write heads for high speed digital tape, etc. because of their high resistively, low dielectric losses, mechanical hardness, high Curie temperature and chemical stability [1–4]. Many synthetic approaches have been employed to prepare magnetic nanocrystals [5–9]. The nanocrystals obtained usually have a strong tendency to aggregate, which makes it very difficult to exploit their unique physical properties. The amorphous matrixes have been shown to play an important role in retarding the motion of the particles as well as the grain growth during the formation of nanocrystals. Thus dispersed nanocrystals often possess limited particle agglomeration and narrow grain size distribution under the space confinement effects. In addition, the morphologies, particle size distribution and crystal structures for the nanocrystals can be controlled by changing the compositions of the matrixes, concentration and treatment conditions [10].

Yue et al. [11] have reported the effect of molar ratio of metal nitrates to citric acid on the combustion process of NiCuZn ferrite. According to their study, the combustion rate can be controlled by changing the ratio of nitrates to citric acid in starting solutions. Thus, the particle size of NiCuZn ferrite powder depends on the ratio of metal nitrates to citric acid. Similar studies of varying acid to metal ion ratios were performed for citric acid-assisted synthesis of $LiNi_{0.8}Co_{0.2}O_2$ [12], which resulted in decreased in capacity values with higher acid to metal ion ratios. However, the spin dynamics and magnetic properties of the materials synthesized with varying acid to metal ion ratios have not been reported. Electron paramagnetic resonance (EPR) and superconducting quantum interference device (SQUID) are powerful tool in investigation of spin dynamics and magnetic properties in solids. From the EPR and SQUID spectra, we can obtain detailed

*Corresponding author. Fax: +886-3-389-1519.
E-mail address: khwu@ccit.edu.tw (K.H. Wu).

0022-4596/$ - see front matter © 2004 Elsevier Inc. All rights reserved.
doi:10.1016/j.jssc.2004.05.019

information on electronic and magnetic state. The magnetic properties of composite are affected not only by the compositions, additives and annealing conditions but also by the raw materials [13,14]. The magnetic properties of a magnetic material depend largely on the particle size distributions as the domain structure and magnetization process depends on particle size.

In our previous papers [15,16], NiZn ferrite doped with silica powder were prepared using sol–gel auto-combustion method. The spectroscopic characterization, thermal behavior of the formation processes of NiZn ferrite/SiO_2 nanocomposite and the magnetic interaction between silica and NiZn ferrite were studied. According to our study, the content of silica powder in the starting solution affects the combustion process, the interaction between NiZn ferrite and silica, and the particle size of NiZn ferrite. The present paper describes the synthesis of SiO_2-doped NiZn ferrite nanocomposites by hydrolysis of tetraethoxysilane (TEOS) onto NiZn ferrite particle and the effect of varying the citric acid to metal nitrates ratio R on the structural and magnetic properties. The spectroscopic characterization, crystallite sizes, EPR parameters (ΔH_{PP}, g factor, N_S and T_2) and SQUID parameters (M_s, M_r and H_c) of composites are studied using FTIR, ^{29}Si CP/MAS NMR, XRD, EPR and SQUID.

2. Experimental

2.1. Preparation of NiZn ferrite/SiO_2 composite

Analytical grade nickel nitrate, zinc nitrate, iron nitrate, citric acid and TEOS were used as raw materials to prepare $Ni_{0.5}Zn_{0.5}Fe_2O_4$/20 wt% SiO_2 nanocomposite. The ferrite powder was synthesized as follows. The initial molar ratio was Ni:Zn:Fe = 1:1:4. First, 2.0 g $Ni(NO_3)_2 \cdot 6H_2O$, 2.05 g $Zn(NO_3)_2 \cdot 6H_2O$ and 11.12 g $Fe(NO_3)_3 \cdot 9H_2O$ were dissolved in 20 mL of ethanol, and then 20 wt% of TEOS and H_2O in a molar ratio of 1:4 was added into the solution. The acid to metal nitrates molar ratio R values was varied at 0.7, 1 and 1.2 with similar synthesis conditions. A small amount of ammonia was added to the solution to adjust the pH value to about 5. The entire mixture was thoroughly stirred for 24 h at room temperature. Then, the mixed solution was poured into a teflon dish and heated 12 h at 60°C and 3 h at 100°C under a vacuum to obtain a dried gel. When ignited at any point, the dried gel burnt in a self-propagating combustion manner until all the gels were burnt out completely to form a loose powder.

2.2. Characterization of NiZn ferrite/SiO_2 composite

Infrared spectra (IR) of the gel precursor and the as-burnt powder were recorded on a Bomem DA 3.002 spectrophotometer from 400 to 4000 cm^{-1} by the KBr pellet method. The solid-state ^{29}Si-NMR spectra of the gel precursor and the as-burnt powder were determined using a Bruker MSL-400 with the cross-polarization combined with magic angle spinning (CP/MAS). The ^{29}Si CP/MAS NMR provides a unique way to follow the structure of silica network and the magnetic interaction between iron (III) and silica. The phase identification of the gel precursor and the as-burnt powder was performed using X-ray diffraction (XRD) with CuK_α radiation. Average grain sizes (D) were determined from the XRD peaks using Scherrer's formula. The electron paramagnetic resonance (EPR) spectra of the composites were recorded on a Bruker EMX-10 spectrometer operating at X-band ($v = 9.6$ GHz) with 100 kHz field modulations. DPPH ($g = 2.0036$) was used as a field marker. The EPR spectra were recorded at variable temperatures (200–400 K) using variable temperature controller. Magnetization measurements were performed in fields of up to 5 T using a Quantum Design SQUID magnetometer (Model MPMS5).

3. Results and discussion

3.1. Phase analysis and particle size of powder

Fig. 1 shows X-ray diffraction (XRD) patterns of the dried gel and as-burnt powders. The XRD of the dried gel powder (Fig. 1d) shows characteristic lines for silica standard, Fe_2O_3 and FeO(OH) [17]. All the as-burnt powders are a single phase NiZn ferrite with a spinel structure. This result indicates that the NiZn ferrites are directly formed after auto-combustion of gels. The direct transformation of crystalline ferrite from amorphous gel during combustion is surely due to the greater heat generated from the exothermic reaction of nitrates

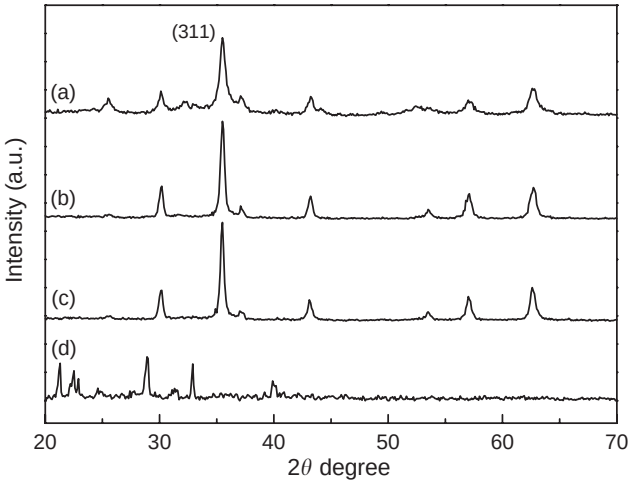

Fig. 1. XRD spectra of NiZn ferrite/SiO_2 with (a) $R = 0.7$, (b) $R = 1.0$, (c) $R = 1.2$, and (d) the dried nitrate–citrate–SiO_2 gel ($R = 1.0$).

and citric acid [15]. Crystallite sizes of the composite are calculated from the X-ray peak broadening of the (311) diffraction peak using Scherrer's formula [11]:

$$D = 0.9\lambda/\beta\cos\theta, \quad (1)$$

where D is the crystallite size in nm, λ the radiation wavelength (0.154056 nm for CuK_α), β the bandwidths at half-height, and θ the diffraction peak angle. The calculated crystallite sizes are 14, 19, and 22 nm, respectively, for NiZn ferrite/20 wt% SiO_2 with $R =$ 0.7, 1.0, and 1.2. The crystallite size was found to be the lowest for the composites synthesized with $R = 0.7$. The result is due to the interaction between NiZn ferrite crystallites with silica and the interaction reduces NiZn ferrite agglomeration.

3.2. Infrared spectra

FTIR spectra provide evidence for the formation of ferrite. Fig. 2 shows the IR spectra of the dried gel and as-burnt powder. All the dried gels show characteristic vibration of nitrate–citrate precursors and silica. The bands at about 3150, 1614 and 1394 cm^{-1}, corresponding to the O–H group of citric acid, carboxylate anion, and anti-symmetric NO_3^- stretching vibration, respectively (Fig. 2a) [15]. The silica network is characterized by the strong absorptions at 3500, 1088, and 474 cm^{-1}, corresponding to the silanol groups (Si–OH), Si–O–Si anti-symmetric stretch and bending mode. It is evident from the Figs. 2b–d that the broad bands at 958 and 880 cm^{-1} corresponding to the Si–O–Fe and Si–OH stretching vibrations, which decrease with increasing R value. The result indicates a more Si–OH groups and magnetic interaction between the NiZn ferrite and silica at $R = 0.7$. A new band appears at 568–582 cm^{-1} in the spectra of the as-burnt powder, which is the characteristic band of NiZn ferrite [15]. The ferrite-stretching band is shifted to higher wave number as the R value decreased. The results can be ascribed to the formed and enhanced magnetic interaction between the NiZn ferrite and silica through Si–O–Fe bonds [6]. On the other hand, the disappearance or decrease at 1614 and 1394 cm^{-1} of the as-burnt powder reveals that carboxylate and NO_3^- ions take part in the reaction during combustion. Therefore, the combustion can be considered as a thermally induced anionic redox reaction of the gel wherein the citrate ion acts as a reductant and the NO_3^- ion acts as an oxidant [12].

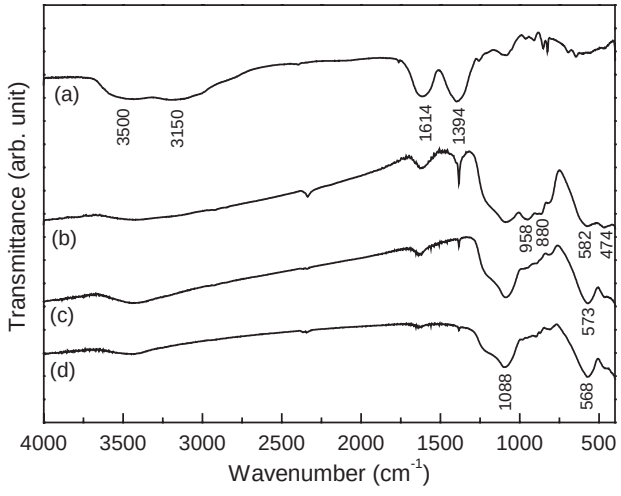

Fig. 2. IR spectra of (a) the dried nitrate–citrate-SiO_2 gel and NiZn ferrite/SiO_2 with (b) $R = 0.7$, (c) $R = 1.0$, and (d) $R = 1.2$.

3.3. ^{29}Si CP/MAS NMR spectra

The ^{29}Si CP/MAS NMR spectra are collected for the dried nitrate–citrate–silica gel and as-burnt powder as shown in Fig. 3. The dried nitrate–citrate–silica gels show characteristic absorptions of silica network at about −92, −100 and −110 ppm corresponding to Q^2, Q^3 and Q^4 structural units, respectively. However, the signals of Q^i in the dried gels are partially overlapped and the intensities were weakened with decreasing R value. This indicates that a more three-dimensional silica network develops at a higher R and hence the magnetic interaction between the NiZn ferrite and silica through Si–O–Fe bonds decreases. On the other hand, there are no signals for the as-burnt powder in Fig. 3d. The disappearance of silica signals between −90 and −110 ppm for NiZn ferrite/SiO_2 composite is due to dipolar interactions between ^{29}Si nuclei and the paramagnetic Fe(III) cation, which provide efficient NMR relaxation sinks. Since Fe(III) cation has a d^5 electronic configuration, there will be five unpaired electron in the d-orbitals of the composite. This fact further reveals that a magnetic ferrite is formed from the as-burnt powder.

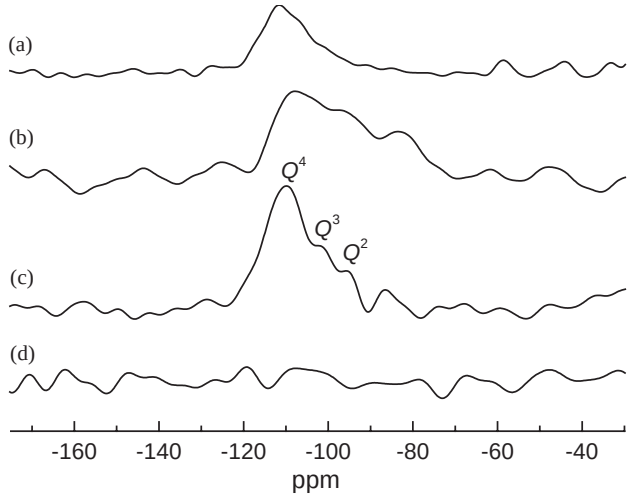

Fig. 3. ^{29}Si NMR spectra of the dried nitrate–citrate–SiO_2 gel synthesized with (a) $R = 0.7$, (b) $R = 1.0$, (c) $R = 1.2$, and (d) NiZn ferrite/SiO_2 ($R = 1.0$).

3.4. Effect of R value on the EPR spectra

The EPR spectra of $Ni_{0.5}Zn_{0.5}Fe_2O_4/SiO_2$ nanocomposites have been recorded at room temperature and the dependence of R value is shown in Fig. 4. The EPR parameters (ΔH_{PP}, g factor, N_S and T_2) obtained from Fig. 4 are given in Table 1. It can be observed that the EPR spectra show a broad signal, the overlap for the broad signal associated with the free or interactive $Ni_{0.5}Zn_{0.5}Fe_2O_4$ clusters with silica was gradually discriminated. Moreover, the EPR parameters (i.e., ΔH_{PP}, g factor, and N_s) of composites increase with increasing R value (Table 1). The results are due to the increased particle size of $Ni_{0.5}Zn_{0.5}Fe_2O_4$ with increasing R value. This could make the dipole–dipole interactions in $Ni_{0.5}Zn_{0.5}Fe_2O_4$ particles increase, and then increase of ΔH_{PP}, g factor and N_s [18].

The spin–spin relaxation process is the energy difference (ΔE) transferred to neighboring electrons and the relaxation time (T_2) can be determined from the peak-to-peak linewidth according to:

$$\frac{1}{T_2} = \frac{g\beta\Delta H_{1/2}}{\hbar}, \Delta H_{1/2} = \sqrt{3}\Delta H_{PP} \quad (2)$$

(in s^{-1}), where β is the Bohr magneton (9.274×10^{-21} erg G^{-1}), $\Delta H_{1/2}$ the linewidth (in G) at half-height of the absorption peak, and $\hbar$ a constant (1.054×10^{-27} erg s) [19]. In our case T_2 decreases with increasing R value, indicating that the spin relaxation at low R value exhibit a slow relaxation and a fast relaxation at high R value. The result may be due to the motion of ferrites is restricted by agglomeration at $R = 1.2$. Thus, the T_2 increases with decreasing particle size as shown in Table 1 leading to the decrease of the ΔH_{PP}.

3.5. Temperature dependence EPR spectra

Typical EPR spectra of the $Ni_{0.5}Zn_{0.5}Fe_2O_4$/20 wt% SiO_2 ($R = 1.0$) composite showed broad signals in the temperature range of 200–400 K, as shown in Fig. 5. The spectra are in general asymmetric in nature. It is found that the point of minimum derivative ($H_0 = 3400$ G) remains nearly constant throughout the temperature range, while the peak-to-peak amplitude increases and the point of maximum derivative right shift with increasing temperature. On the other hand, the overlap for the broad signal associated with the free or interactive $Ni_{0.5}Zn_{0.5}Fe_2O_4$ clusters with silica was gradually indistinct with increase in temperature. The increased temperature should increase the motion of electrons, causing stronger superexchange interactions between the magnetic ions through oxygen ions and a decrease in ΔH_{PP}.

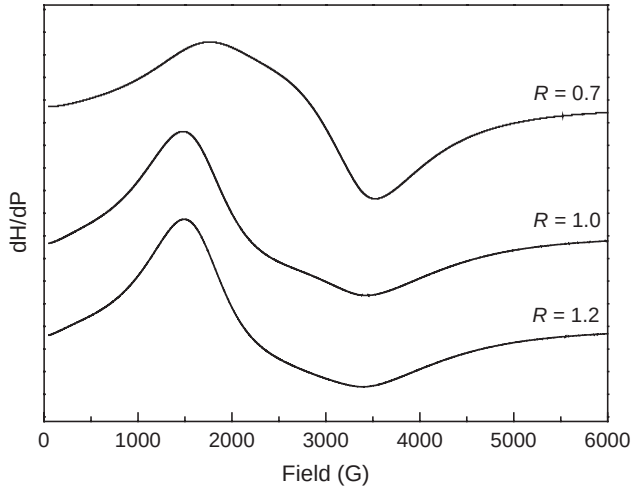

Fig. 4. EPR spectra of NiZn ferrite/SiO_2 synthesized at different acid to metal nitrate ratios R.

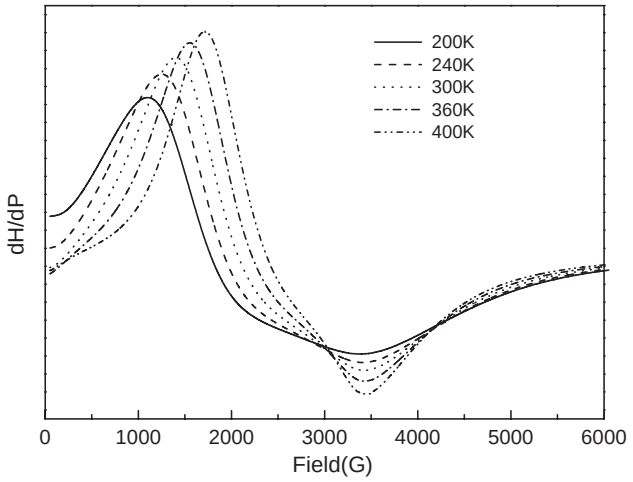

Fig. 5. Typical temperature-dependent EPR spectra of NiZn ferrite/SiO_2 with $R = 1.0$.

Table 1
EPR and SQUID characteristics of $Ni_{0.5}Zn_{0.5}Fe_2O_4/SiO_2$ composites with different R value at room temperature[a]

Sample	D (nm)	ΔH_{PP} (G)	g facter	N_S ($\times 10^{10}$ spins g^{-1})	T_2 ($\times 10^{-11}$ s)	M_s (emu/g)	M_r (emu/g)	H_c (G)
$R = 0.7$	14	1740	2.31	5.60	2.40	11	6.9	70
$R = 1.0$	19	1911	3.40	6.74	1.47	22	6.3	70
$R = 1.2$	22	1942	3.46	6.84	1.42	26	2.3	70

[a] D is the crystallite size, ΔH_{PP} the peak-to-peak linewidth, N_S the spin number, T_2 the spin–spin relaxation time, M_s the saturation magnetization, M_r the remnant magnetization, and H_c the coercivity.

Fig. 6 shows the variation in the peak-to-peak linewidth (ΔH_{PP}) with temperature. The values of ΔH_{PP} continuously decrease with increase in temperature. This is due to the fact that in a randomly oriented dispersed ferromagnet the absorption linewidth turns out to be a non-monotonic function of temperature. At low temperature, the linewidth is large due to the scatter in direction of anisotropic field of particles. As the temperature increases, the tendency to make magnetic moment isotropic causes linewidth to decrease [20]. The energy between two adjacent degenerate spin energy levels ΔE has the same behavior of the linewidth. The reduction of linewidth may cause a reduction in the separate energy ΔE. The value of ΔE is given by the relation $\Delta E = h\nu = g\beta H_0$ [19]. Thus, the g value is defined as the constant of proportionality between the frequency and the field at which resonance occurs, and is proportional to the magnetic moment of the molecule being studied. Fig. 7 shows the variation in the g factor

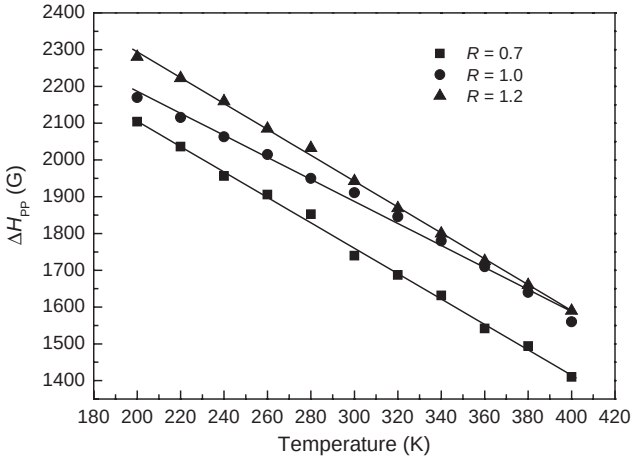

Fig. 6. The linewidth (ΔH_{PP}) as a function of temperature of NiZn ferrite/SiO_2 composites obtained for varying R value.

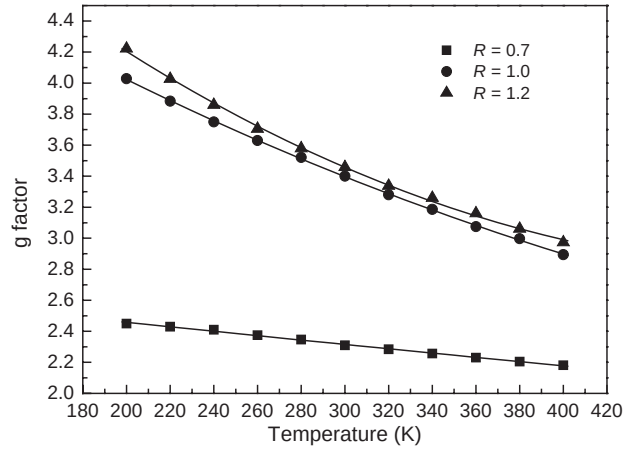

Fig. 7. The g factor as a function of temperature of NiZn ferrite/SiO_2 composites obtained for varying R value.

with temperature of the $Ni_{0.5}Zn_{0.5}Fe_2O_4$/20 wt% SiO_2 composites. It was observed that g value decreases with increasing temperature. The weakening of magnetic moment is responsible for the observed reduction in the g factor [21]. On the other hand, the g factor of composite at $R = 0.7$ is less affected by temperature, while the g factor deviates from the linear behavior for the temperature range of 200–400 K at $R = 1.0$ and 1.2. The observation may be due to the decreased crystallization degree of $Ni_{0.5}Zn_{0.5}Fe_2O_4$ particles at a lower R. This could make the dipole interactions decrease, and then give a small g factor.

The spin–spin relaxation T_2 can be easily measured from the peak-to-peak EPR linewidth ΔH_{PP} and g factor according to the Eq. (2). The temperature dependence of T_2 value in the NiZn ferrite/SiO_2 composites with different R value is shown in Fig. 8. Magnetic dipole interactions among particles and superexchange interactions between the magnetic ions though oxygen ions are two predominant factors that determine the EPR resonance parameters, g factor and ΔH_{PP}. Strong dipole interactions give a large ΔH_{PP} and g factor; further, strong superexchange interactions produce a small ΔH_{PP} and g factor [22]. The increased temperature should increase the motion of electrons, causing stronger superexchange interactions among the cations through oxygen ions and a decrease in ΔH_{PP} and g factor. Therefore, the T_2 value increases with increasing temperature.

3.6. Squid magnetometry measurements

The magnetic properties of NiZn ferrite/SiO_2 nanocomposites are dictated by the superexchange couplings between the magnetic ions via oxygen anions [13]. The magnetic properties of the composites depend on the microstructure and measuring parameters such as particle size, porosity and magnetizing frequency.

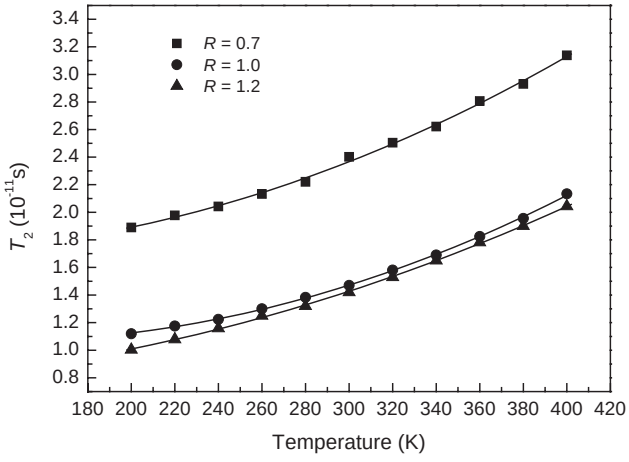

Fig. 8. The spin–spin relaxation time (T_2) as a function of temperature of NiZn ferrite/SiO_2 composites obtained for varying R value.

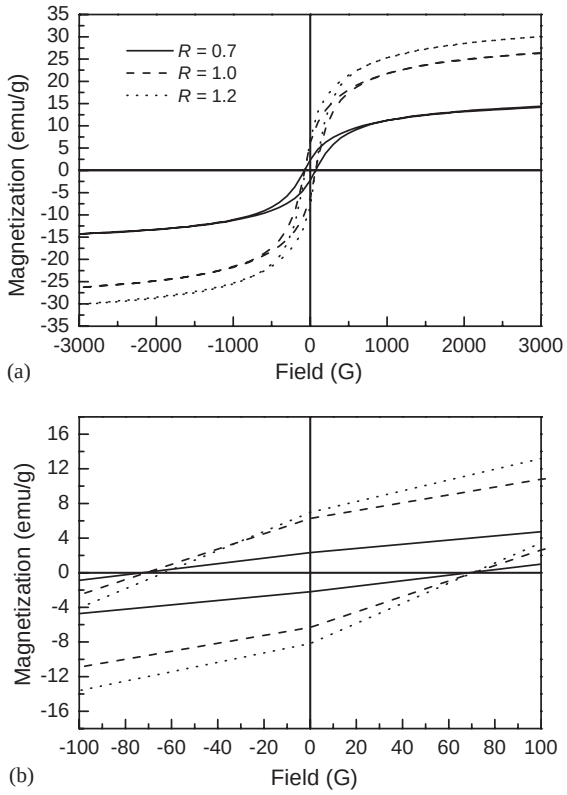

Fig. 9. The magnetic hysteresis loops of NiZn ferrite/SiO_2 composites with different R value (a), and low-field range (b).

Fig. 9 shows the magnetic hysteresis loops of NiZn ferrite/SiO_2 nanocomposites with different R value at room temperature. The hysteresis loops were measured to determine parameters such as the saturation magnetization (M_s), remnant magnetization (M_r) and coercivity (H_c), as shown in Table 1. The magnetic properties of the samples clearly depend on the size of the nanocrystallites. It is evident from the Fig. 9 that the saturation magnetization (M_s) increases with increasing R value, while the coercivity (H_c) remains constant. The increase in saturation magnetization (M_s) and decrease in remnant magnetization (M_r) can be attributed to an increase of the mean size of nanocrystallites [14].

4. Conclusions

Variations in the structural and magnetic properties of the NiZn ferrite/SiO_2 nanocomposites synthesized at different acid to metal nitrates ratio R revealed that increasing the R value has a direct effect on the formation of the composite and its magnetic properties. Increasing the R value resulted in a decrease in interaction between $Ni_{0.5}Zn_{0.5}Fe_2O_4$ and SiO_2 increased the magnetic dipolar interactions existing among the fine clusters $Ni_{0.5}Zn_{0.5}Fe_2O_4$ and increased the particle size. Further, increasing the R value resulted in an increase in ΔH_{PP}, g factor and N_S, while the T_2 decreased. The observation can be accounted due to the increase of the dipole–dipole interactions existing among the Ni–Zn ferrite. The variations in the EPR parameters (ΔH_{PP}, g factor, N_S and T_2) with temperature were shown that ΔH_{PP}, g factor and N_S decreased and T_2 increased with increasing temperature. The results may be due to the enhanced superexchange interaction, which induced the decrease in ΔH_{PP}, g factor, N_S and increase in T_2. The results of SQUID, measured at room temperature, show that M_s increased and M_r decreased with increasing R value. The observation can be accounted due to an increase of mean size of the nanocrystallites.

Acknowledgments

The authors thank the National Science Council of the Republic of China (Grant NSC 92-2113-M-014-002). Authors wish to express their gratitude to Miss J.C. Chen of NSC Instrument Center for EPR analysis.

References

[1] J.B. da Silva, N.D.S. Mohallem, J. Magn. Magn. Mater. 226–230 (2001) 1393.
[2] A.M. Abden, J. Magn. Magn. Mater. 185 (1998) 199.
[3] K.I. Arshak, A. Ajina, D. Egan, Microelectron. J. 32 (2001) 113.
[4] X.D. Tong, B. Xue, Y. Sun, Biotech. Prog. 17 (2001) 134.
[5] D. Ravinder, K.V. Kumar, Mater. Lett. 49 (2001) 57.
[6] G.S. Li, L.P. Li, R.L. Smith Jr., H. Inomata, J. Mol. Struct. 560 (2001) 87.
[7] V.M. Bujoreamu, E. Segal, Solid State Sci. 3 (2001) 407.
[8] J. Plocek, A. Hutlova, D. Niznansky, J. Bursik, J.L. Rehspringer, Z. Micka, J. Non-Crystalline Solids 315 (2003) 70.
[9] C. Caizer, M. Popovici, C. Savii, Acta Materialia 51 (2003) 3607.
[10] C. Pascal, J.L. Pascal, F. Favier, M.L.E. Moubtassim, C. Payen, Chem. Mater. 11 (1999) 141.
[11] Z. Yue, L. Li, J. Zhou, H. Zhang, Z. Gui, Mater. Sci. Eng. B 64 (1999) 68.
[12] G. Ting-Kuo Fey, R.F. Shiu, V. Subramanian, C.L. Chen, Solid State Ionics 148 (2002) 291.
[13] Y. Choi, H.S. Shim, J.S. Lee, J. Alloys Compd. 326 (2001) 56.
[14] C. Caizer, Mater. Sci. Eng. B 100 (2003) 63.
[15] K.H. Wu, Y.C. Chang, G.P. Wang, J. Magn. Magn. Mater. 269 (2004) 150.
[16] K.H. Wu, Y.C. Chang, H.B. Chen, C.C. Yang, D.N. Horng, J. Magn. Magn. Mater. 278 (2004) 156.
[17] J.B. da Silva, N.D.S. Mohallem, J. Magn. Magn. Mater. 226–230 (2001) 1393.
[18] X. Li, G. Lu, S. Li, J. Alloys Compd. 235 (1996) 150.
[19] J.F. Raber, Experimental Methods in Polymer Chemistry-Physical Principal and Applications, Wiley, New York, 1980, p. 332.
[20] R. Massart, D. Zins, F. Gendron, M. Rivoire, R.V. Mehta, R.V. Upadhyay, P.S. Goyal, V.K. Aswal, J. Magn. Magn. Mater. 201 (1999) 73.
[21] P. Kinnari, R.V. Upadhyay, R.V. Mehta, J. Magn. Magn. Mater. 252 (2002) 35.
[22] L. Li, G. Li, R.L. Smith, H. Inomata, Chem. Mater. 12 (2000) 3705.